J Mater Sci (2020) 55:3107–3117

Metals & corrosion

Wettability, interfacial reactions, and impact strength of Sn–3.0Ag–0.5Cu solder/ENIG substrate used for fluxless soldering under formic acid atmosphere

Siliang He[1,2,*], Runhua Gao[1,2], Yu-An Shen[2], Jiahui Li[1,2], and Hiroshi Nishikawa[2]

[1] *Graduate School of Engineering, Osaka University, Suita, Osaka 565-0871, Japan*
[2] *Joining and Welding Research Institute, Osaka University, Ibaraki, Osaka 565-0047, Japan*

Received: 14 August 2019
Accepted: 23 October 2019
Published online:
30 October 2019

© Springer Science+Business Media, LLC, part of Springer Nature 2019

ABSTRACT

Fluxes have a negative impact on the environment; as a result, fluxless soldering has become a promising method in electronic packaging. However, detailed studies on fluxless soldering are very rare, especially those involving the use of electroless nickel immersion gold (ENIG) substrate under formic acid (FA) atmosphere that can effectively reduce the majority of solders. In this work, the characteristic parameters of FA reflow soldering performed by combining Sn–3.5Ag–0.5Cu (SAC305) solder and ENIG substrate are compared with the soldering conducted using liquid rosin mildly activated (RMA) flux. It is found that the wettability of FA-exposed solder is greater than that of RMA-containing solder because the former spreads across the interfacial layer of intermetallic compounds (IMCs) produced before the melting of SAC305. Additionally, the interfacial reactions of FA-exposed solder resemble those of RMA solder before and after the thermal aging at 150 °C. Therefore, the impact strengths of these two solders are almost the same due to the similarity of their microstructures and close growth rates of $(Cu,Ni)_6Sn_5$ IMC layers during thermal aging. The findings of this study suggest that FA reflow soldering is a promising environmentally friendly technique for electronic packaging.

Introduction

Sn-rich solders with good wettability and low melting points (210–220 °C) are commonly used for soldering interconnections in the surface mount technology, flip chip, and micro-bump methods utilized in advanced electronic packaging [1–6]. During the soldering process, flux serves as a chemical cleaning agent that not only removes the oxide layer, but also enhances the wettability between the molten solder and the substrate [7]. After soldering, flux residues are typically removed to prevent corrosion [8, 9]; however, the use of halogenated solvents (such as chlorofluorocarbons [10]) for removing rosin-

Address correspondence to E-mail: q40770606@gmail.com

https://doi.org/10.1007/s10853-019-04153-9

based liquid fluxes must be limited due to its negative impact on the environment [11]. Meanwhile, in modern electronics, the increase in the solder bump density and reductions in the gap between the chip and substrate gap and the spaces between various components can become roadblocks for the flux cleaning process [12]. Additionally, solder pastes with the newly developed no-clean type fluxes suffer from the flux residue splattering on in-circuit testing pads [13], which decrease the optical efficiency of optoelectronic products (including light emitting diodes) [8, 10, 14, 15]. Consequently, fluxless soldering demonstrated high market potential [10] and received much attention from researchers, especially fluxless soldering using an ultrasonic technology [16–19], plasma-assisted dry soldering [20], a fluxless process using argon atom sputter—etching [19], and fluxless Au/Sn eutectic die bonding in vacuum [21].

One commonly used fluxless soldering method involves the decrease in the oxidation state of metals and enhancement of solder wettability in a reducing atmosphere, such as hydrogen gas or formic acid (FA; HCOOH). On the one hand, the efficient reduction by pure hydrogen at 300 °C is not suitable for most solders utilized in the electronics industry [7, 8, 12, 15, 22–25]. On the other hand, among many possible interconnecting materials, the applicability of lead-free Sn–Ag–Cu alloy (SAC solder with $> 95\%$ Sn) in microelectronics packaging continues to grow [5, 26, 27]. The oxide phase of SAC solder is composed of SnO and SnO_2 compounds [28–30], whose reactions with FA can be expressed as follows [25]:

$$SnO + 2HCOOH \rightarrow Sn(HCOO)_2 + H_2O \quad (1)$$

$$SnO_2 + 2HCOOH \rightarrow Sn(HCOO)_2 + O_2 + H_2 \quad (2)$$

Sn-(II) formate ($Sn(HCOO)_2$) decomposes into Sn, carbon dioxide, and hydrogen at 150 °C according to the following reaction:

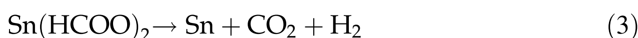

$$Sn(HCOO)_2 \rightarrow Sn + CO_2 + H_2 \quad (3)$$

Furthermore, the contact angle of SAC solder with a typical intermetallic compound (IMC) layer formed at the interface between the solder and Cu substrate during FA reflow soldering is almost equal to that observed for the liquid rosin mildly activated flux (RMA solder) [31]. Hence, FA is a promising reagent for fluxless soldering.

To prevent oxidation and ensure a relatively long pre-assembly shelf life, electroless nickel immersion gold (ENIG) layers are deposited on Cu substrates. ENIG exhibits good wettability with SAC during soldering, and its Ni layer serves as a diffusion barrier against the reaction of Cu with Sn-rich solders inducing the growth of brittle IMCs during electromigration and thermal aging [32–34]. Despite these advantages, the effect of FA reflow soldering on the ENIG substrate and mechanisms of its interfacial reactions have not been investigated in detail.

In this study, SAC solder balls were applied onto ENIG substrates under FA atmosphere, and their wettability and interfacial reactions were examined. Because the mechanical reliability of solder joints is a critical parameter in the electronics industry [35, 36], impact tests were conducted on these joints before and after the thermal aging at 150 °C for 168, 512, and 1008 h. In addition, RMA reflow soldering was performed for comparison purposes.

Experimental

Solder wettability

A Sn–3.0massAg–0.5massCu solder (SAC solder) ball with a diameter of 0.76 mm and a Cu substrate with the dimensions 30 mm × 30 mm × 0.5 mm and ENIG finish (ENIG substrate) were prepared for wettability testing, as shown in Fig. 1. FA gas (5 vol% formic acid + 95 vol% N_2) was used as soldering reducing atmosphere for the fluxless soldering process. The thermal effect observed during the remelting of the solder ball (reflow) on the wettability of FA-exposed solder was investigated at various temperatures ranging from 250 to 290 °C, as shown in

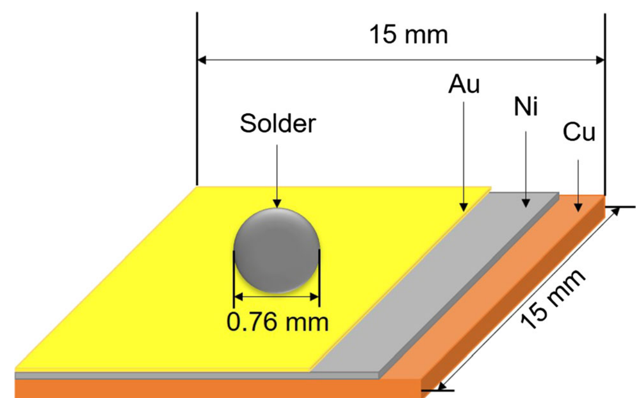

Figure 1 Schematic diagram of ENIG pads using for wettability test.

Table 1. Spreading areas were measured by an optical microscope (OM, KEYENCE VHX-900) after soldering. In situ observations were conducted as second-by-second measurements of the spreading areas using a charge-coupled device (CCD) camera (SONY) to evaluate the corresponding spreading rates. (Both these parameters were utilized to determine solder's wettability.) The exact values of solder spreading areas were calculated using commercial software (ImageJ).

Interfacial reactions and impact testing

Solder bumps (consisting of the SAC solder balls on ENIG pads embedded into a flame retardant-4 (FR-4) substrate as shown in Fig. 2) were used for studying interfacial reactions and impact strengths via a reflow process. (The corresponding reflow profile is shown in Fig. 3.) To obtain ENIG substrates, electroless Ni layers with thicknesses of 5 μm were deposited onto Cu pads. (The thickness of the Au flash on the Ni layer was approximately 50 nm.) Before the reflow process, the SAC solder balls were immersed in a 4 vol% HCl solution for 120 s, after which both the balls and FR-4 ENIG substrates were ultrasonically cleaned in ethanol for 300 s. After the reflow, the solder bumps were aged inside an oil bath at 150 °C for 168, 512, and 1008 h.

To estimate the impact strengths of the soldered bumps, high-speed tests were conducted using a micro-impact tester (MI-S, Yonekura Mfg. Co., Ltd.). The testing speed was 1 m/s, and the impact height from the solder resist was equal to 0.08 mm (Fig. 4). Ten bumps were evaluated under each condition using the average value of the impact strength.

Cross-sectional microstructures of the solder bumps were observed by a field-emission scanning electron microscope (FE-SEM, Hitachi SU-70), and their IMC thicknesses were determined. Elemental compositions of the solder bumps were identified by field-emission electron probe microanalysis (EPMA, JEOL JXA-8530F).

Table 1 Summary of FA-exposed solder heating processes for wettability test

Heating process	①	②	③
Preheat temperature (°C)	110	110	110
Preheat time (s)	60	60	60
Peak temperature (°C)	250	270	290
Peak time (s)	120	120	120
Heating rate (°C/s)	2.5	2.5	2.5

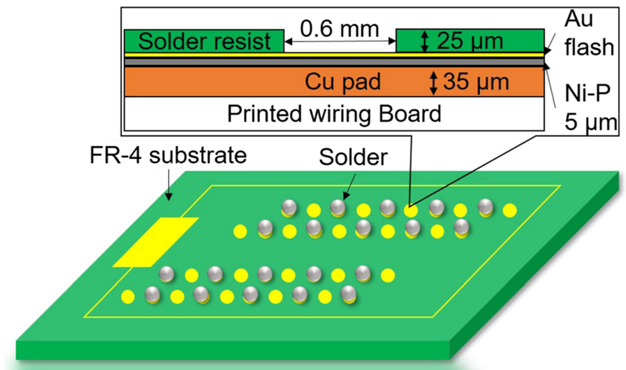

Figure 2 Schematic diagram of Cu substrate with ENIG finish using for soldering process.

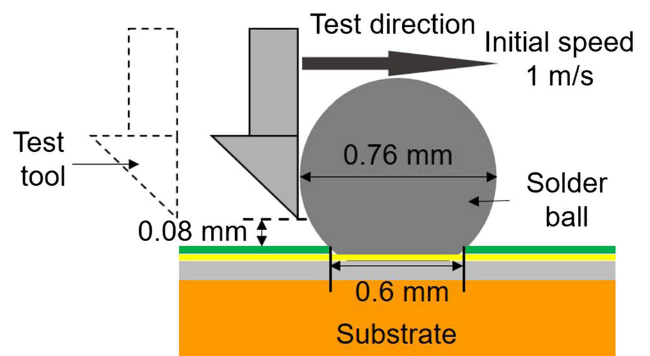

Figure 3 Schematic diagram of high-speed impact test.

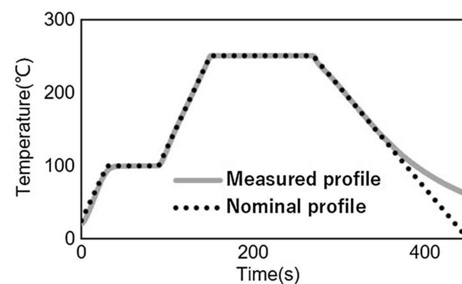

Figure 4 Soldering process of RMA solder.

Results and discussion

Wettability

Figure 5a shows the average spreading areas obtained for FA-exposed solder at 250 °C, 270 °C, and 290 °C after 2 min and for the solder containing RMA flux at 250 °C corresponding to the reflow

temperature of SAC solder joints [31, 37, 38]. The average spreading area in the former case was 31.19 mm^2, and that in the second case was 28.43 mm^2. Moreover, the average spreading areas of FA-exposed solder during the reflows at 270 °C and 290 °C were 37.44 and 40.77 mm^2, respectively. The obtained results show that the average spreading area of FA-exposed solder exhibits a positive correlation with the reflow temperature under the specified conditions, which significantly improves solder's wettability [39, 40] because the viscosity and surface tension of liquid Sn-based solders typically demonstrate negative correlations with temperature unless the latter is extremely high [41, 42]. Figure 5b shows the spreading rates obtained for FA-exposed and RMA solders after 120 s of the reflow at 250 °C. The observed trends are very similar, while the spreading area of FA-exposed solder is slightly larger than that of the solder with RMA flux. The spreading areas of both solders gradually increased even in the end of the reflow process, which was in good agreement with the results of a previous study [43]. The reason for the enhanced wettability of the solder exposed to FA atmosphere is the formation of an IMC layer before solder melting. In the experiment conducted according to the diagram presented in Fig. 6, a glass pad with a Sn bulk on its surface was placed on the left side, and an ENIG pad was placed at a distance of 1 mm from the glass pad on the right side. Subsequently, both pieces were placed inside a reflow chamber. After introducing FA atmosphere, the chamber was heated to 250 °C for 30 min.

After the reaction, Sn residues were formed on the ENIG pad near the glass substrate, as shown in Fig. 7a. Because the boiling point of Sn (about 2602 °C) is much higher than 250 °C, we believe that the volatilization of Sn barely occurs under this condition. Hence, the Sn residues were likely caused by the Sn formate steaming ($Sn(COOH)_{i(g)}$) from the left side (Sn/glass) to the right side (ENIG) before the Sn phase melted on the glass surface [44] followed by the Sn formate ($Sn(COOH)_{i(s)}$) decomposition on the ENIG substrate at a temperature of around 200 °C [44–47]. The latter was formed during the reduction process under FA atmosphere ($iHCOOH_{(g)}$) via the chemical reactions:

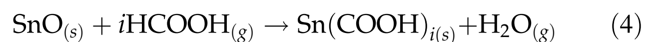

$$SnO_{(s)} + iHCOOH_{(g)} \rightarrow Sn(COOH)_{i(s)} + H_2O_{(g)} \quad (4)$$

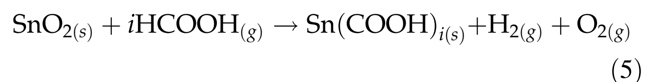

$$SnO_{2(s)} + iHCOOH_{(g)} \rightarrow Sn(COOH)_{i(s)} + H_{2(g)} + O_{2(g)} \quad (5)$$

Further, the Sn reacted with FA as follows:

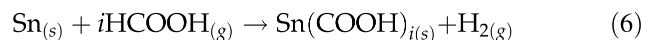

$$Sn_{(s)} + iHCOOH_{(g)} \rightarrow Sn(COOH)_{i(s)} + H_{2(g)} \quad (6)$$

After that, Sn formate evaporated:

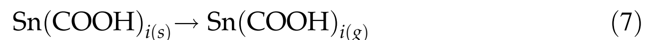

$$Sn(COOH)_{i(s)} \rightarrow Sn(COOH)_{i(g)} \quad (7)$$

The formation process of Sn residues on the ENIG substrate via Sn formate steaming is illustrated in Fig. 7b, while the surface modification caused by

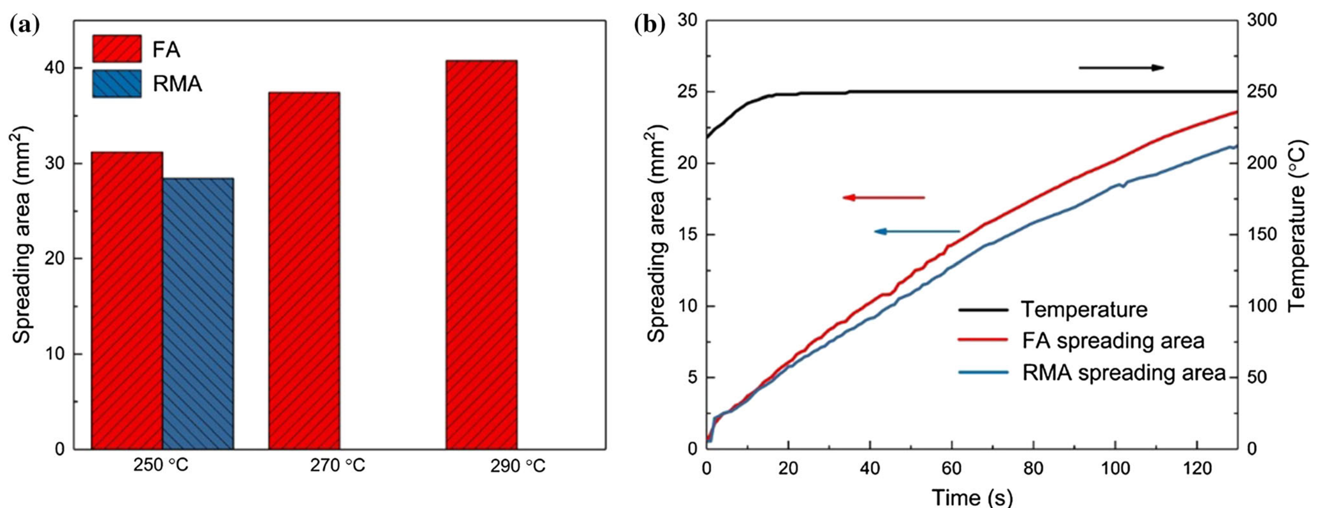

Figure 5 Spreading area of solders on ENIG pad: **a** the average spreading areas of solders under formic acid atmosphere at 250 °C, 270 °C, and 290 °C for 2 min, and that of solder using RMA flux was at 250 °C and **b** the tendency of the spreading of solder under formic acid atmosphere and solder using RMA flux of reflow at 250 °C.

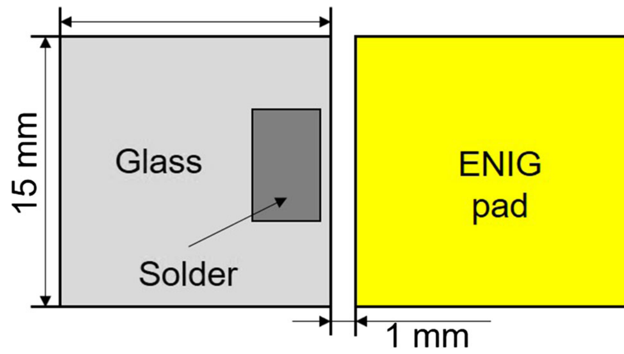

Figure 6 Schematic diagram of Sn steaming experiment.

their melting is depicted in Fig. 7c. The modified surface with a composition determined by EPMA contained 57.39 at% Sn, 30.68 at% Ni, and 11.93 at% Au. As the reflow temperature (250 °C) was greater than the Sn melting point (232 °C), we assumed that the surface modification was caused by the formation of IMCs (Ni_3Sn_4 and $AuSn_4$) [32, 48]. Therefore, during soldering under FA atmosphere, Sn formate produced from solid Sn spread across the ENIG substrate around the SAC305 solder ball (see Fig. 8a) and then decomposed into Sn on the ENIG substrate at approximately 200 °C (Fig. 8b). As the temperature increased above 232 °C, the SAC solder ball and decomposed Sn melted and formed IMCs at the interface (Fig. 8c). Owing to the IMC formation via the reaction between the decomposed Sn and ENIG substrate, the molten solder ball could spread across the surface of IMCs (Fig. 8d).

In general, the wetting of a solder on a particular substrate produces a typical reactive wetting system [49], in which IMCs precipitate at the liquid/solid interface [50]. According to the reaction product control (RPC) model, reaction products determine the ultimate solder wettability and spreading process [51]. In this study, although the same $(Cu,Ni)_6Sn_5$ layer was formed and contacted the liquid solder, the solder wettability under FA atmosphere was greater than that of the solder containing RMA flux. In previous studies, it was found that the wettability of lead-free solder on the IMC layer (Cu_6Sn_5/Cu_3Sn) was higher than that of the same solder on the Cu surface [49, 52, 53]. In addition, the wettability of Sn on the Ag_3Sn IMC surface was greater than that of Sn on an Ag substrate [54]. Thus, it can be concluded that the higher wettability of FA-exposed solder as compared with that of the solder containing RMA flux is caused by the spreading of the SAC solder ball on the IMC surface. Meanwhile, the surface roughness was also changed by the formation of IMCs under FA atmosphere, which significantly affected solder's wettability [48, 55–58]. Hence, a detailed study of the effects produced by the surface tension-driven flow (such as Sn steaming) on the surface morphology under FA atmosphere is required.

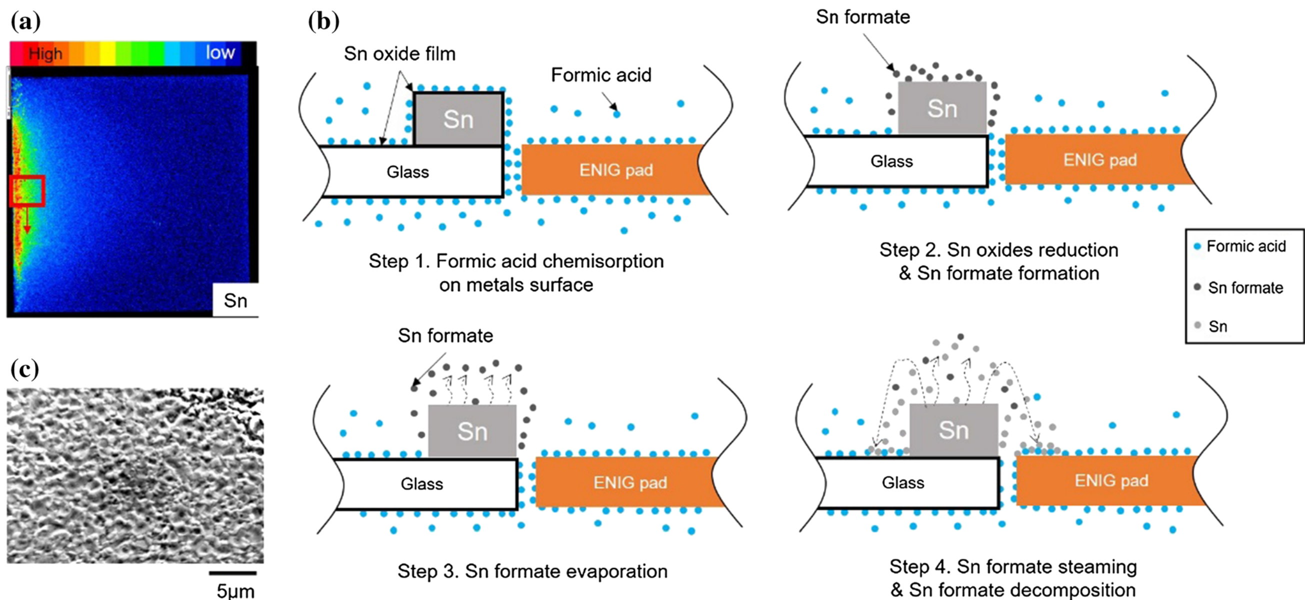

Figure 7 Diagram of Sn steaming hypothesis: **a** EPMA mapping results of Sn steaming experiment; **b** the process of Sn residues on the ENIG substrate via Sn formate steaming hypothesis; and **c** SEM image of IMC in the area of Sn residues.

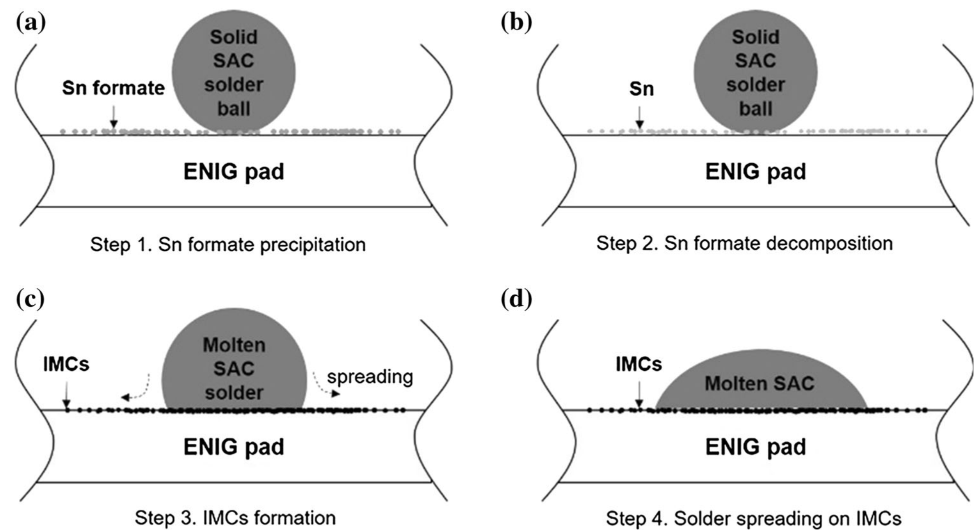

Figure 8 Effect of Sn steaming phenomenon on wettability.

Moreover, we also found that under the same conditions, the spreading rate of FA-exposed solder on the Cu substrate was much lower than that of the solder containing RMA flux (Fig. 9). This difference was likely caused by the continuous breakdown of the Cu oxide film, which could not be easily removed by the reaction with FA and thus reduced the solder wettability. Therefore, the wettability of FA-exposed solder on the ENIG pad was significantly greater than that of the same solder on the Cu substrate

Interfacial reactions

Figure 10a shows the SEM image of the joint cross section obtained for as-reflowed FA soldering. After the reflow process, the Au flash layer dissolved into the molten SAC305 solder, leaving $(Cu,Ni)_6Sn_5$ IMC at the interface between SAC305 solder and the Ni(P) layer. Moreover, a thin Ni_3P layer was produced between the $(Cu,Ni)_6Sn_5$ IMC and Ni(P) layers. The Cu phase of the former layers resulted from SAC305 solder, and its composition determined by EPMA corresponded to 42.60 at% Cu, 16.50 at% Ni, and 40.90 at% Sn. According to the results of thermodynamic calculations, $(Cu,Ni)_6Sn_5$ was formed by the dissolution of Ni in the Cu_6Sn_5 phase because the reflow time was not sufficient for the formation of a ternary compound $Ni_{26}Cu_{29}Sn_{45}$ [59]. Consequently, $(Cu,Ni)_6Sn_5$ was produced at the interface instead of Cu_6Sn_5 or Ni_3Sn_4 [60]. Furthermore, a P-rich Ni layer was also formed between the $(Cu,Ni)_6Sn_5$ and Ni–P layers; it contained approximately 25 at% P suggesting Ni_3P as its possible composition [32]. Ni(P) species were crystallized into Ni_3P ones because the self-crystallization temperature of amorphous Ni(P) was 250 °C [60]. After the thermal aging for 1008 h, the thickness of the $(Cu,Ni)_6Sn_5$ layer increased (Fig. 10c); moreover, the presence of stable Ni_3P species strongly affected the growth of the Ni–Sn IMC phase [1]. Hung et al. [61, 62] suggested that the Ni_3P layer could act as a barrier to the diffusion of Ni and consequently suppressed the growth of the Ni_3Sn_4 layer. Additionally, the interfacial morphologies of RMA solder before (Fig. 10b) and after (Fig. 10d) the thermal aging were almost identical to those of FA-exposed solder. Figure 11 shows that the IMC growth rate during FA reflow soldering was almost equal to that during RMA

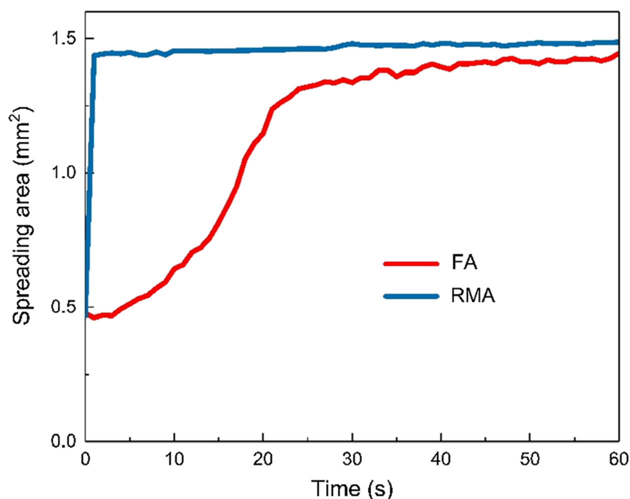

Figure 9 Tendency of the spreading of FA-exposed solder and RMA solder on Cu pad reflowed at 250 °C.

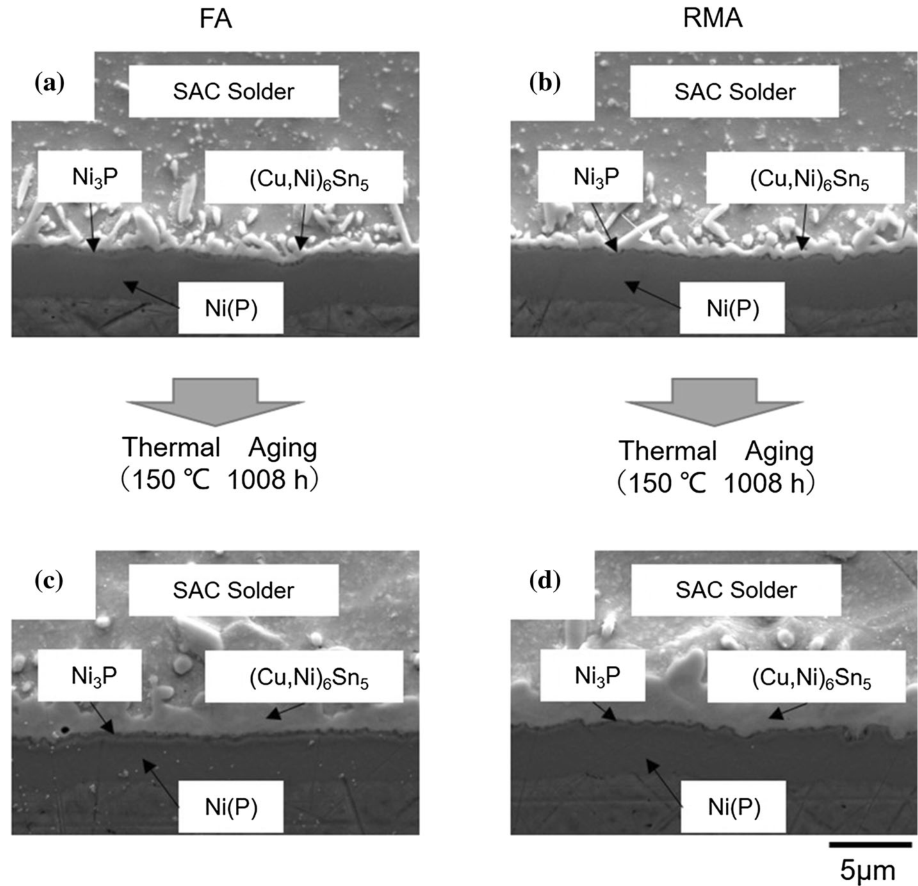

Figure 10 Cross-sectional SEM image of solder bumps on ENIG substrate for FA soldering and RMA soldering: **a**, **b** as -reflowed solder bumps; **c**, **d** thermally aged solder bumps.

reflow soldering at different aging times, and that the thickness of the IMC layer was proportional to the square root of the aging time, indicating that FA atmosphere barely affected the interfacial reaction between the ENIG substrate and SAC solder. From the results presented above, it can be concluded that FA reflow soldering is a promising alternative to RMA reflow soldering in terms of performance and environmental characteristics, although no reliability testing of the former method has been conducted yet.

Impact strength

The mechanical reliability of FA reflow soldering was evaluated by performing impact tests, and the obtained data were compared with the results of RMA reflow soldering (Fig. 12). During FA reflow soldering, the impact strength before the thermal aging at 150 °C was 107 MPa, and its magnitude decreased to 86, 83, and 80 MPa after the thermal aging for 168, 504, and 1008 h, respectively. All impact strengths of the samples used for FA reflow soldering were slightly higher than those of the

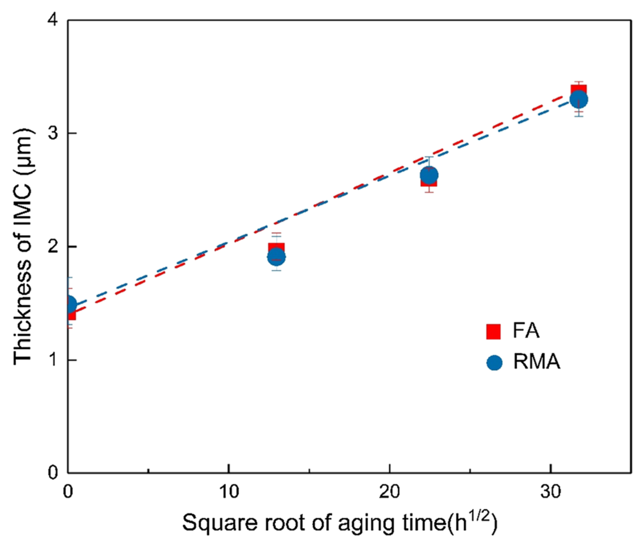

Figure 11 Statistics of IMC thickness of solder bumps for FA soldering and RMA soldering.

specimens utilized for RMA reflow soldering, and their decreases were likely caused by the growth of brittle IMCs at the interface during thermal aging. Figure 13 shows the EPMA mappings, corresponding

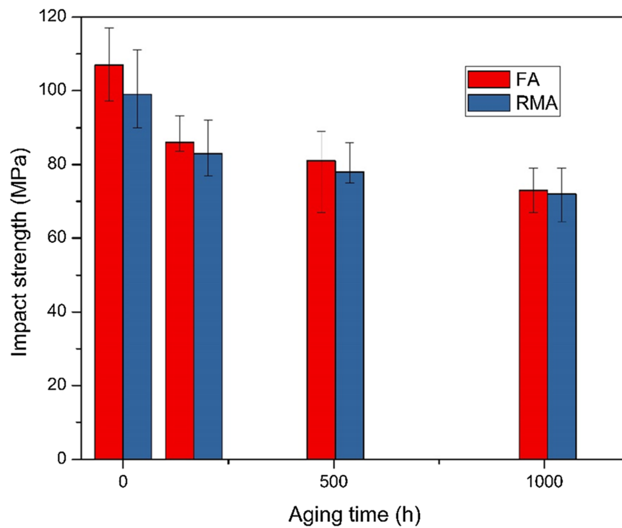

Figure 12 Effect of aging time on impact strength of FA-exposed and RMA solder bumps.

to the SEM images of the fracture surfaces obtained for the FA-exposed and RMA solders before and after the thermal aging for 1008 h. (Here, the impact direction is oriented from left to right.) In the as-reflowed solders, as the high concentration of Ni remained in the left section of the fracture surface, fracture mostly occurred across the IMC layer, while the high concentrations of Sn and Ag were partially preserved in the right section. The joints of both the as-reflowed FA-exposed and RMA solders cracked along the solder/substrate interface and then propagated into the bulk solder. After the thermal aging for 1008 h, high contents of Ni were observed across the entire fracture surface, while Sn and Cu species were also detected in the same areas for both cases, suggesting that the fracture occurred within the IMC layer at the solder/substrate interface after thermal aging for 1008 h. It was reported previously that ductile fracture occurred in the solder bulk where brittle fracture originated in the IMC layer [36]. Therefore, the as-reflowed solders exhibited both ductile and brittle fractures simultaneously. After 1008 h of aging, the fracture mode changed to the total brittle fracture with an increase in thickness of the IMC layer. Because the differences in the impact strengths and fracture modes of FA-exposed and

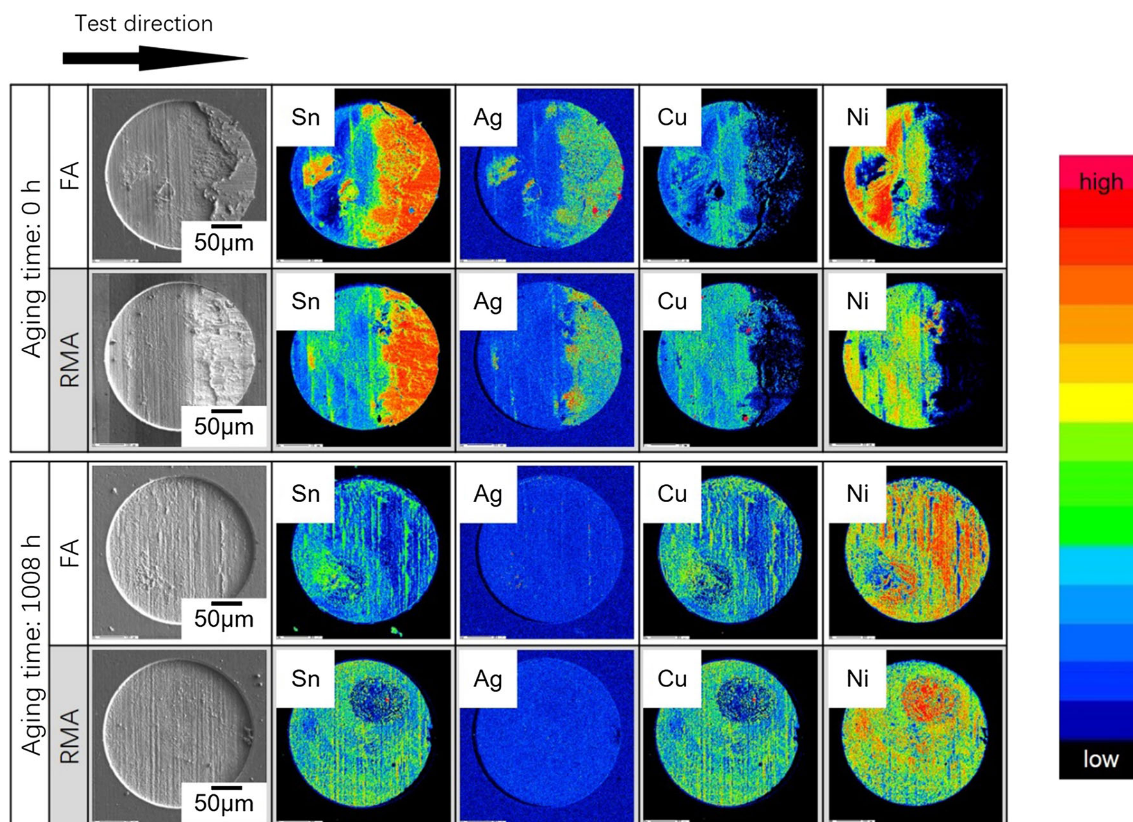

Figure 13 EPMA mapping analysis results of fracture surface of as-reflowed and 1008 h aged FA-exposed and RMA solders in impact test.

RMA solders were very small, FA atmosphere had almost no effect on their mechanical stabilities. Hence, the latter factor can be neglected when considering the replacement of RMA reflow soldering with FA reflow soldering.

Conclusion

In this study, the wettability, interfacial reactions, and impact strength of FA-exposed solder on the ENIG substrate were examined, and the obtained results were compared with the parameters of RMA reflow soldering. As indicated by in situ observations, the spreading area of the solder exposed to FA atmosphere was 10% greater than that of the solder containing RMA flux, which demonstrated the enhancement of solder's wettability by FA. The latter was caused by the solder spreading on the interfacial layer of $(Cu,Ni)_6Sn_5$ IMC formed by Sn residues on the ENIG substrate via Sn formate steaming before the solder ball melted during FA reflow soldering. The IMC growth rate of FA-exposed solder was nearly identical to that of RMA solder, and their interfacial reactions were very similar. Moreover, the impact strength of FA-exposed solder (107 MPa) was approximately equal to that of RMA solder (99 MPa) due to the same interfacial reactions. The decrease in the impact strength observed after 168, 504, and 1008 h of the thermal aging at 150 °C was induced by the growth of the brittle IMC layer at the interface with a similar pattern. The findings of this work indicate that RMA reflow soldering can be potentially replaced with FA reflow soldering for the environmental protection during electronic packaging.

Acknowledgements

The authors would like to acknowledge SANYO-SEIKO, LTD (Japan) for the financial support of this study.

Funding

This study was funded by the Project to Create Research and Educational Hubs for Innovative Manufacturing in Asia, Osaka University under the Special Project of the Ministry of Education, Culture, Sports, Science and Technology (MEXT).

Compliance with ethical standards

Conflict of interest The authors declare that they have no conflicts of interest.

References

[1] Kotadia HR, Howes PD, Mannan SH (2014) A review: on the development of low melting temperature Pb-free solders. Microelectron Reliab 54:1253–1273

[2] Lee N-C (1999) Lead-free soldering-where the world is going. Adv Microelectron 26:29

[3] Kang SK, Sarkhel AK (1994) Lead (Pb)-free solders for electronic packaging. J Electron Mater 23:701–707

[4] Wood E, Nimmo K (1994) In search of new lead-free electronic solders. J Electron Mater 23:709–713

[5] Suganuma K (2001) Advances in lead-free electronics soldering. Curr Opin Solid State Mater Sci 5:55–64

[6] Shen Y-A, Chen C (2017) Effect of Sn grain orientation on formation of Cu_6Sn_5 intermetallic compounds during electromigration. Scripta Mater 128:6–9

[7] He S, Nishikawa H (2017) Effect of substrate metallization on the impact strength of Sn–Ag–Cu solder bumps fabricated in a formic acid atmosphere. In: International conference on electronics packaging (ICEP) (IEEE), pp 381–385

[8] Hanss A, Hutter M, Trodler J, Elger G (2016) In: Electronic components and technology conference (ECTC), 2016 IEEE 66th (IEEE), pp 447–454

[9] Bušek D et al (2016) Flux effect on void quantity and size in soldered joints. Microelectron Reliab 60:135–140

[10] Lin W, Lee Y (1999) Study of fluxless soldering using formic acid vapor. IEEE Trans Adv Packag 22:592–601

[11] Lu Q-B, Sanche L (2001) Effects of cosmic rays on atmospheric chlorofluorocarbon dissociation and ozone depletion. Phys Rev Lett 87:078501

[12] Samson M et al (2016) In: 2016 IEEE 66th electronic components and technology conference (ECTC) (IEEE), pp 574–579

[13] Dušek K, Bušek D (2016) Problem with no-clean flux spattering on in-circuit testing pads diagnosed by EDS analysis. Microelectron Reliab 56:162–169

[14] Hanss A, Schmid M, Bhogaraju SK, Conti F, Elger G (2018) In: 2018 International conference on electronics packaging and iMAPS all Asia conference (ICEP-IAAC) (IEEE), pp 479–484

[15] Hanss A, Elger G (2018) Residual free solder process for fluxless solder pastes. Solder Surf Mt Technol 30:118–128

[16] Koleňák R, Kostolný I, Drápala J, Sahul M, Urminský J (2018) Characterizing the soldering alloy type In–Ag–Ti and the study of direct soldering of SiC ceramics and copper. Metals 8:274–291

[17] Koleňák R, Kostolný I, Kusý M (2018) Characterization of soldering alloy type Zn–In–Mg and the study of direct soldering of silicon and copper. Mater Sci Eng A 712:302–312

[18] Hong S-M, Kang C-S, Jung J-P (2002) Fluxless Sn-3.5 mass% Ag solder bump flip chip bonding by ultrasonic wave. Mater Trans 43:1336–1340

[19] Nishikawa T et al (1999) In: 1994 Proceedings of 44th electronic components and technology conference (IEEE), pp 286–292

[20] Koopman N, Bobbio S, Nangalia S, Bousaba J, Piekarski B (1993) In: Proceedings of IEEE 43rd electronic components and technology conference (ECTC'93) (IEEE), pp 595–605

[21] Lee CC, Chen Y-C, Matijasevic G, Metzler R (1994) In: 1994 Proceedings of 44th electronic components and technology conference (IEEE), pp 595–599

[22] Humpston G, Jacobson DM (2004) Principles of soldering. ASM International, Cleveland

[23] Dong C, Arslenian G (1996) Fluxless soldering of flip chip assemblies. Nepcon West, pp 96–112

[24] Dong CC, Schwarz A, Roth DV (1997) Feasibility of fluxless reflow of lead-free solders in hydrogen and forming gas. Nepcon Malays 97:03–32

[25] Monta M, Okiyama K, Sakai T, Imaizumi N (2012) In: 2012 IEEE 14th electronics packaging technology conference (EPTC) (IEEE), pp 602–607

[26] Cheng S, Huang C-M, Pecht M (2017) A review of lead-free solders for electronics applications. Microelectron Reliab 75:77–95

[27] Lu D, Wong C (2009) Materials for advanced packaging, vol 181. Springer, New York

[28] Zhang S, Zhang Y, Wang H (2009) Effect of oxide thickness of solder powders on the coalescence of SnAgCu lead-free solder pastes. J Alloys Compd 487:682–686

[29] Chang H, Chen H, Li M, Wang L, Fu Y (2009) Generation of Tin (II) oxide crystals on lead-free solder joints in deionized water. J Electron Mater 38:2170–2178

[30] Batzill M, Diebold U (2005) The surface and materials science of tin oxide. Prog Surf Sci 79:47–154

[31] Siliang H, Hiroshi N (2017) Effect of thermal aging on the impact strength of soldered bumps under formic acid atmosphere. Q J Jpn Weld Soc 35:127s–131s

[32] Yoon J-W, Jung S-B (2005) Interfacial reactions between Sn–0.4 Cu solder and Cu substrate with or without ENIG plating layer during reflow reaction. J Alloys Compd 396:122–127

[33] Liu X, Nishikawa H (2017) Pressureless sintering bonding using hybrid microscale Cu particle paste on ENIG, pure Cu and pre-oxidized Cu substrate by an oxidation–reduction process. J Mater Sci: Mater Electron 28:5554–5561

[34] Lee H et al (2018) Effect of solder resist dissolution on the joint reliability of ENIG surface and Sn–Ag–Cu solder. Microelectron Reliab 87:75–80

[35] Date M, Shoji T, Fujiyoshi M, Sato K, Tu K (2004) Ductile-to-brittle transition in Sn–Zn solder joints measured by impact test. Scripta Mater 51:641–645

[36] Wang J, Nishikawa H (2014) Impact strength of Sn–3.0 Ag–0.5 Cu solder bumps during isothermal aging. Microelectron Reliab 54:1583–1591

[37] Shen Y-A, Lin C-M, Li J, He S, Nishikawa H (2019) Effect of FeCoNiCrCu 0.5 high-entropy-alloy Substrate on Sn grain size in Sn–3.0 Ag–0.5 Cu solder. Sci Rep 9:3658–3664

[38] Shen Y-A, Ouyang F-Y, Chen C (2019) Effect of Sn grain orientation on growth of Cu–Sn intermetallic compounds during thermomigration in Cu–Sn_2. 3Ag–Ni microbumps. Mater Lett 236:190–193

[39] Matsumoto T, Nogi K (2008) Wetting in soldering and microelectronics. Annu Rev Mater Res 38:251–273

[40] Suganuma K, Niihara K, Shoutoku T, Nakamura Y (1998) Wetting and interface microstructure between Sn–Zn binary alloys and Cu. J Mater Res 13:2859–2865

[41] Lee JH, Lee DN (2001) Use of thermodynamic data to calculate surface tension and viscosity of Sn-based soldering alloy systems. J Electron Mater 30:1112–1119

[42] Zhao N, Pan X, Yu D, Ma H, Wang L (2009) Viscosity and surface tension of liquid Sn–Cu lead-free solders. J Electron Mater 38:828–833

[43] Kim P, Tu K (1996) Morphology of wetting reaction of eutectic SnPb solder on Au foils. J Appl Phys 80:3822–3827

[44] Conti F, Hanss A, Mokhtari O, Bhogaraju SK, Elger G (2018) Formation of tin-based crystals from SnAgCu alloy under formic acid vapor. New J Chem 42:19232–19236

[45] Mokhtari O et al (2019) Characterization of tin-oxides and tin-formate crystals obtained from SnAgCu solder alloy under formic acid vapor. New J Chem 43:10227–10231

[46] Conti F, Hanss A, Fischer C, Elger G (2016) Thermogravimetric investigation on the interaction of formic acid with solder joint materials. New J Chem 40:10482–10487

[47] He S, Gao R, Li J, Shen Y-A, Nishikawa H (2019) In-situ observation of fluxless soldering of Sn–3.0Ag–0.5Cu/Cu under a formic acid atmosphere. Mater Chem Phys. https://doi.org/10.1016/j.matchemphys.2019.122309

[48] Yoon J-W, Noh B-I, Jung S-B (2010) Effects of third element and surface finish on interfacial reactions of Sn–Ag–xCu (or Ni)/(Cu or ENIG) solder joints. J Alloys Compd 506:331–337

[49] Kumar G, Prabhu KN (2007) Review of non-reactive and reactive wetting of liquids on surfaces. Adv Coll Interface Sci 133:61–89

[50] Lin Q, Li F, Wang J (2018) Wetting of Sn/Cu and Sn/Cu–Sn IMCs at 623–723K. J Alloys Compd 767:877–882

[51] Eustathopoulos N (2005) Progress in understanding and modeling reactive wetting of metals on ceramics. Curr Opin Solid State Mater Sci 9:152–160

[52] Liu C, Kim H, Tu K, Totta P (1996) Dewetting of molten Sn on Au/Cu/Cr thin-film metallization. Appl Phys Lett 69:4014–4016

[53] Wang H, Zhao H, Sekulic DP, Qian Y (2008) A comparative study of reactive wetting of lead and lead-free solders on Cu and (Cu_6 Sn_5/Cu_3 Sn)/Cu substrates. J Electron Mater 37:1640–1647

[54] Liashenko O, Hodaj F (2017) Wetting and spreading kinetics of liquid Sn on Ag and Ag_3Sn substrates. Scripta Mater 127:24–28

[55] He B, Lee J, Patankar NA (2004) Contact angle hysteresis on rough hydrophobic surfaces. Colloids Surf A 248:101–104

[56] Chen Y, He B, Lee J, Patankar NA (2005) Anisotropy in the wetting of rough surfaces. J Colloid Interface Sci 281:458–464

[57] Quéré D (2002) Rough ideas on wetting. Physica A 313:32–46

[58] Nakae H, Inui R, Hirata Y, Saito H (1998) Effects of surface roughness on wettability. Acta Mater 46:2313–2318

[59] Kim K, Huh S, Suganuma K (2003) Effects of intermetallic compounds on properties of Sn–Ag–Cu lead-free soldered joints. J Alloys Compd 352:226–236

[60] Kim D, Pak JJ (2010) Micro void growth in NiSnP layer between $(Cu,Ni)_6$ Sn_5 intermetallic compound and Ni_3 P by higher reflow temperature and multiple reflow. J Mater Sci: Mater Electron 21:1337–1345

[61] Hung K, Chan Y, Tang C, Ong H (2000) Correlation between Ni_3 Sn_4 intermetallics and Ni_3 P due to solder reaction-assisted crystallization of electroless Ni–P metallization in advanced packages. J Mater Res 15:2534–2539

[62] Hung K, Chan Y, Tang C (2000) Metallurgical reaction and mechanical strength of electroless Ni–P solder joints for advanced packaging applications. J Mater Sci: Mater Electron 11:587–593

Publisher's Note Springer Nature remains neutral with regard to jurisdictional claims in published maps and institutional affiliations.